

This document is confidential and is proprietary to the American Chemical Society and its authors. Do not copy or disclose without written permission. If you have received this item in error, notify the sender and delete all copies.

Towards the Microscopic Identification of Anions and Cations at the Ionic Liquid | Ag(111) Interface: A Combined Experimental and Theoretical Investigation

Journal:	<i>ACS Nano</i>
Manuscript ID:	Draft
Manuscript Type:	Article
Date Submitted by the Author:	n/a
Complete List of Authors:	Buchner, Florian; Helmholtz Institute Ulm - Electrochemical Energy Storage, ; Ulm University, Institute of Surface Chemistry and Catalysis Tonigold, Katrin; Helmholtz Institute Ulm - Electrochemical Energy Storage, ; Ulm University, Institute of Theoretical Chemistry Uhl, Benedikt; Helmholtz Institute Ulm - Electrochemical Energy Storage, ; Ulm University, Institute of Surface Chemistry and Catalysis alwast, dorothea; Helmholtz Institute Ulm - Electrochemical Energy Storage, Wagner, Nadja; Helmholtz Institute Ulm - Electrochemical Energy Storage, ; Ulm University, Institute of Surface Chemistry and Catalysis Groß, Axel; Helmholtz Institute Ulm - Electrochemical Energy Storage, ; Ulm University, Institute of Theoretical Chemistry Behm, R. Jürgen; Helmholtz Institute Ulm - Electrochemical Energy Storage, ; Ulm University, Institute of Surface Chemistry and Catalysis

SCHOLARONE™
Manuscripts

1
2
3
4
5
6
7
8
9
10
11
12
13
14
15
16
17
18
19
20
21
22
23
24
25
26
27
28
29
30
31
32
33
34
35
36
37
38
39
40
41
42
43
44
45
46
47
48
49
50
51
52
53
54
55
56
57
58
59
60

Towards the Microscopic Identification of Anions and Cations at the Ionic Liquid | Ag(111) Interface: A Combined Experimental and Theoretical Investigation

Florian Buchner,^{‡,a,b} Katrin Forster-Tonigold^{‡,a,c}, Benedikt Uhl,^{a,b} Dorothea Alwast,^{a,b}

*Nadja Wagner,^{a,b} Axel Groß^{a,c}, and R. Jürgen Behm^{*a,b}*

^[a] Helmholtz Institute Ulm - Electrochemical Energy Storage, Albert-Einstein-Allee 11,
D-89081 Ulm,

^[b] Ulm University, Institute of Surface Chemistry and Catalysis, Albert-Einstein-Allee 47,
D-89081 Ulm,

^[c] Ulm University, Institute of Theoretical Chemistry, Albert-Einstein-Allee 11, D-89081 Ulm

Prof. Dr. R. J. Behm
Universität Ulm
Institut für Oberflächenchemie und Katalyse
Albert-Einstein-Allee 47
D-89069 Ulm, Germany
Phone: +49 (0)731/50-25451
Fax: +49 (0)731/50-25452
E-Mail: juergen.behm@uni-ulm.de

[‡] These authors contributed equally

1
2
3 ABSTRACT

4 The interaction between an adsorbed 1-butyl-1-methylpyrrolidinium
5 bis(trifluoromethylsulfonyl)imide [BMP][TFSA] ionic liquid (IL) layer and a Ag(111)
6 substrate, under ultrahigh vacuum (UHV) conditions, was investigated in a combined
7 experimental and theoretical approach, by high-resolution scanning tunneling microscopy
8 (STM) and dispersion corrected density functional theory calculations (DFT-D). Most
9 important, we succeeded in unambiguously identifying cations and anions in the adlayer by
10 comparing experimental images with submolecular resolution and simulated STM images
11 based on DFT calculations. Different adlayer phases include a mobile 2D liquid phase at room
12 temperature and two 2D solid phases at around 100 K, i.e., a 2D glass phase with short-range
13 order and some residual, but very limited mobility and a long-range ordered 2D crystalline
14 phase. The mobility in the different adlayer phases, including melting of the 2D crystalline
15 phase, was evaluated by dynamic STM imaging. The DFT-D calculations show that the
16 interaction with the substrate is composed of mainly van der Waals and weak electrostatic
17 (dipole-induced dipole) interactions, and that upon adsorption most of the charge remains at
18 the IL, leading to attractive electrostatic interactions between the adsorbed species.
19
20
21
22
23
24
25
26
27
28
29
30
31
32
33
34
35
36
37

38 KEYWORDS: Ionic liquids, scanning tunneling microscopy, density functional theory,
39
40 surface chemistry, self-assembly, molecule-molecule and molecule-substrate
41
42 interactions
43
44

45 **Submitted to ACS Nano, .RECEIVED DATE (...)**

46
47
48 TITLE RUNNING HEAD: Identification of anions and cations of an ionic liquid adlayer on
49
50 Ag(111)
51
52
53
54
55
56
57
58
59
60

1. Introduction

Ionic liquids (ILs), which are molten salts usually consisting of organic ions with a melting point below 100°C,^{1,2} have attracted considerable interest in recent years because of their unusual physicochemical properties such as high ionic conductivity and electrochemical stability, very low vapor pressure, or low flammability. Due to the large variety of combinations of different anion-cation pairs, the properties of the ILs can be adjusted over a wide range, making them highly interesting molecular building blocks for both fundamental research and specific applications.¹⁻⁴ One very interesting application is their use as solvent in electrochemical energy storage, where ionic liquids could replace standard solvents in lithium ion and lithium air batteries.⁵⁻⁸ They are also discussed as support-modifying functional layers in heterogeneous catalysis.^{9,10} For the successful transfer into application, it would be highly desirable to understand the processes at the IL | solid and IL | vacuum interface on a fundamental level, at the molecular scale. As one important point, this includes the various aspects of structure formation of ILs on flat surfaces, as a model for the IL | solid interface.

In this paper we report results of a combined experimental and theoretical study on the adsorption and structure formation behavior of the anion-cation pair 1-butyl-1-methylpyrrolidinium bis(trifluoromethylsulfonyl)imide [BMP][TFSA] on Ag(111) under ultrahigh vacuum (UHV) conditions in the sub-monolayer to monolayer range, applying high resolution scanning tunneling microscopy (STM) and dispersion corrected density functional theory (DFT-D) calculations.¹¹ Despite numerous investigations, conducted both *in situ*, in an electrochemical environment¹²⁻¹⁶ and *ex situ* under UHV conditions,^{9,10,17-27} studies on the interaction of IL monolayers with single crystalline surfaces are rare. Cremer et al. studied the adsorption of 1,3-dimethylimidazolium bis(trifluoromethylsulfonyl)imide [MMIM][TFSA] and 1-methyl-3-octylimidazolium bis(trifluoromethylsulfonyl)imide [OMIM][TFSA] ionic liquid on Au(111) by angle-resolved X-ray photoelectron spectroscopy (ARXPS) and concluded that at a coverage of up to 1.0 ML both anions and cations are in direct contact with

1
2
3 the surface, presumably in an alternating arrangement.²⁸ (Note that the authors of that study
4 defined a coverage of 1 ML as a saturated layer of anions and cations on top of each other,
5 while in the present study we define the coverage by using the number of adsorbed ions at
6 saturation of that layer as reference. This requires to multiply the coverages from the above
7 group by a factor of 2, which is done in the following.) In contrast to the findings for Au(111),
8 they found for [MMIM][TFSA] adsorption on Ni(111) that up to coverages of ~0.80 ML the
9 ions are vertically aligned, with the imidazolium cation directly on the Ni surface and the
10 corresponding anion on top of it.²⁶ By analysing infrared reflection absorption spectroscopy
11 (IRAS) measurements with the help of density functional theory (DFT) calculations, Sobota et
12 al. concluded that at sub-monolayer coverages the adsorption geometry of an imidazolium
13 based IL on Al₂O₃/NiAl(110) is likely to be a *cis*-conformation for [TFSA]⁻ anions, with the
14 SO₂ groups attached to the substrate.²⁹

15
16
17
18
19
20
21
22
23
24
25
26
27
28
29
30 In a very first molecular resolution STM investigation, a short-range ordered structure was
31 resolved for the 1-butyl-1-methylpyrrolidinium tris(pentafluoroethyl)trifluorophosphate
32 [BMP][FAP] ionic liquid on Au(111) under UHV conditions at 200 K.³⁰ Molecular objects in
33 form of dots could be identified, which could be either ion pairs in a double layer arrangement
34 or individual ions, with both ions in contact to the surface. More recently, STM measurements
35 by Foulston et al.³¹ on 1-ethyl-3-methylimidazolium bis(trifluoromethylsulfonyl)imide
36 [EMIM][TFSA] adsorbed on Au(110) resolved molecular entities, which they assumed to
37 consist of closely associated ion pairs. However, in neither of these cases was it possible to
38 distinguish and to molecularly identify anions and cations by STM imaging. For a detailed
39 molecular scale understanding of the processes at the IL | solid interface, this would be highly
40 desirable, together with a similar understanding of the nature of the substrate – adsorbate and
41 adsorbate – adsorbate interactions. This is topic of the present work, where the combination of
42 high resolution STM imaging with sub-molecular resolution and density functional theory
43 based calculations allows for an unambiguous identification of the different adsorbed species
44
45
46
47
48
49
50
51
52
53
54
55
56
57
58
59
60

1
2
3 and gives detailed insight into the bonding situation of the adlayer, including both substrate –
4
5 adsorbate and adsorbate – adsorbate interactions. To the best of our knowledge, this is the first
6
7 time that individual ions could be resolved and identified in an IL adlayer.
8
9

10 11 **2. Methods**

12 13 **2.1 Experimental Methods**

14
15 The STM experiments were performed in a two chamber UHV system, at a background
16
17 pressure in the low 10^{-10} mbar regime. The microscope is an Aarhus type STM (SPECS
18
19 Aarhus STM 150), which allows to measure at variable temperatures between 100 K and
20
21 400 K by cooling with liquid nitrogen and resistive heating. The tunneling current was
22
23 between 20 pA and 150 pA and the applied bias voltage between -0.1 V and -1.5 V referred to
24
25 the sample. The images were recorded in constant current mode. Variable temperature STM
26
27 experiments were conducted with a heating rate of ~ 0.5 K/min. The Ag(111) single crystal
28
29 was purchased from MaTecK, the ionic liquid [BMP][TFSA] from Merck in ultrapure quality.
30
31 Clean Ag(111) surfaces were prepared by Ar^+ -ion sputtering (500 eV) and annealing to 770 K.
32
33 Prior to deposition on Ag(111), [BMP][TFSA] was degassed in UHV for at least 24 hours in a
34
35 previously baked out crucible. The ionic liquid was evaporated onto the Ag substrate held at
36
37 room temperature (RT) with a commercial Knudsen effusion cell for organic molecules
38
39 (Ventiotec, OVD-3), which was heated to 373 K. The evaporation rates were previously
40
41 checked by a quartz micro balance. The sample was cooled down to a temperature of roughly
42
43 100 K in the time span of 2-3 hours before the STM measurements.
44
45
46
47
48

49 50 **2.2 Computational Methods**

51
52 Periodic DFT-calculations were performed using the exchange-correlation functional of
53
54 Perdew, Burke and Ernzerhof (PBE)³² as implemented in the Vienna *ab initio* simulation
55
56 package (VASP).^{33,34} In order to account for dispersive interactions missing in the exchange-
57
58
59
60

1
2
3 correlation functionals of the generalized gradient approximation (GGA), we employed
4
5 Grimme's correction scheme of 2010 (DFT-D3).¹¹ It has recently been shown that this
6
7 approach yields reliable adsorption energies and structures for organic molecules and
8
9 hydrogen-bonded networks on metal surfaces.³⁵⁻³⁷ Ion cores are represented by means of the
10
11 projector augmented wave (PAW) method.^{38,39} The electronic one-particle wave functions
12
13 were expanded in a plane wave basis set up to an energy cut-off of 400 eV.
14
15

16
17 The Ag(111) surface was represented by a slab consisting of 3 metal layers, separated by a
18
19 vacuum region of about 25 Å. To model the adsorption of one cation-anion pair at the surface,
20
21 we chose a Ag(111)-(5x5) overlayer structure with one adsorbed cation-anion pair per unit
22
23 cell. For the integration over the first Brillouin zone a 2x2x1 Monkhorst-Pack k-point mesh⁴⁰
24
25 with a Methfessel-Paxton smearing of 0.1 eV was employed. The geometry of the adsorption
26
27 complex was optimized by relaxing all atoms of the IL pair and the atoms of the uppermost
28
29 layer of the metal surface. Only these atoms were taken into account for the evaluation of
30
31 dispersive interactions.
32
33

34
35 STM simulations are based on the Tersoff-Hamann approximation.⁴¹ Within that model the
36
37 tunneling current is proportional to the local density of states (LDOS) at the surface close to
38
39 the Fermi energy at the position of the tip. Constant-current images are simulated by an
40
41 isosurface of the LDOS integrated between the Fermi energy of the system and the sample
42
43 bias.
44
45

46
47 Isolated molecules have also been calculated using the GAUSSIAN09 code⁴² in connection
48
49 with the atom centered basis set aug-cc-pVTZ.⁴³⁻⁴⁵ For isolated molecules no dispersion
50
51 corrections have been employed.
52
53

54 55 **3. Results and Discussion**

56
57
58
59
60

1
2
3 To begin with, we discuss the adsorption behavior of [BMP][TFSA] on Ag(111) based on
4 large-scale STM images at sub-monolayer and monolayer coverages. STM images recorded at
5 300 K do not allow us to resolve single IL entities. Instead, stripy features appear, which are
6 not observed on the clean Ag(111) surface (SI I). Therefore these features are related to
7 adsorbed IL entities in a 2D gas / 2D liquid adlayer that diffuse rapidly on the time scale of the
8 STM experiment and can therefore not be resolved.⁴⁶⁻⁴⁸ Similar observations were reported by
9 Waldmann et al. for room temperature imaging of [BMP][FAP] ionic liquid adlayer on
10 Au(111)³⁰ and by Foulston et al. for [EMIM][TFSA] on Au(110).³¹

11
12 In Figure 1 we present constant current STM images recorded at sub-monolayer (Figure 1a)
13 and monolayer coverage (Figure 1b) at around 100 K, where a monolayer is defined as the
14 coverage required to completely cover the surface. Figure 1a shows four silver terraces
15 (depicted as *I*, *II*, *III*, *IV*), which are covered with the adsorbed IL species in different ways.
16 On terrace *I*, we find a large, long-range ordered and homogeneous adsorbate phase without
17 any internal domain boundaries. These large ordered domains are solely observed on large
18 silver terraces; small domains or islands of that phase, separated by domain boundaries or
19 other phases, have not been observed. These domains are referred to as an ordered 2D
20 crystalline phase. Note that at large terraces, at least close to the steps, we also observed
21 regions where the IL adsorbates are arranged in a disordered way, which will henceforth be
22 referred to as 2D glass phase. Terrace *II* (Figure 1a), which is only ~10 nm wide, shows an
23 apparently uncovered, adsorbate free region, at least there is no adlayer structure visible,
24 neither ordered nor disordered. Noisy features in the fast scanning direction are again
25 attributed to highly mobile adsorbed species, i.e., also this area is not free of adsorbates. At
26 the left side of terrace *II*, two islands with arbitrary shapes grow from the step. At the present
27 resolution, these islands consist of single dots, which are arranged in a disordered way (see
28 below). Terrace *III* (Figure 1a) shows a larger region covered with a disordered 2D phase,
29
30
31
32
33
34
35
36
37
38
39
40
41
42
43
44
45
46
47
48
49
50
51
52
53
54
55
56
57
58
59
60

1
2
3 which extends from the left to the right step. Finally, terrace *IV* (Figure 1 a) is nearly
4
5 completely filled with the disordered 2D phase.
6

7
8 Successively increasing the coverage (Figure 1b), the 2D crystalline phase is exclusively
9
10 found on the large terraces; in addition, also disordered regions are found on large terraces
11
12 close to the steps. Narrow terraces (~10 nm width) in Figure 1b are now completely filled up
13
14 with the disordered 2D phase. As the influence of the steps is much larger at narrow terraces,
15
16 it is likely that the interaction with these defects is responsible for the formation of the
17
18 disordered 2D phase, inhibiting the ordering process. In large-scale STM images, three
19
20 orientations of the 2D crystalline phase are found (only one orientation per terrace (SI II)),
21
22 whose orientation differs by multiples of 120°. Hence, these domains are rotationally aligned
23
24 with the underlying Ag(111) surface lattice. The observation that large terraces are largely
25
26 occupied by large and homogeneous ordered domains points towards (weakly) attractive
27
28 adsorbate-adsorbate interactions.
29
30

31
32 Next we concentrate on the dynamic behavior of [BMP][TFSA] on Ag(111) at 100 K.
33
34 Figure 2 shows the boundary between an ordered 2D crystalline phase and an adjacent 2D
35
36 liquid phase, which typically appears frizzy (Figure 2a). Such frizzy features are generally due
37
38 to surface mobility at the phase boundary. Even though we used a high tunneling resistance
39
40 ($R_t \sim 2 - 44 \text{ G}\Omega$), we can not totally exclude tip induced effects. Time sequences of STM
41
42 images were acquired and selected images from two series are shown in Figs. 2b and 2c. The
43
44 time interval from image to image was ~25 s in Figure 2a and ~6 s in Figure 2b. The main
45
46 finding is that the interior of the domain remains stable over time, while the location of the
47
48 phase boundary changes gradually. This behavior can be explained by a 2D adsorption-
49
50 desorption equilibrium at the phase boundary. The IL entities in the 2D liquid phase are highly
51
52 mobile and can not be resolved.⁴⁶⁻⁴⁸
53
54
55
56
57
58
59
60

1
2
3 Dynamic STM measurements were also performed at regions of the surface where both the
4 ordered 2D crystalline phase and the disordered 2D phase coexisted. Selected images
5 extracted from the time lapse movie (see SI III) are shown in Figure 3. On the right terrace,
6 the features in the ordered 2D crystalline phase remain highly stable over time. As in Figure
7 1a, disordered regions are found close to the step. On the left terrace, the STM time sequence
8 shows that an apparently uncovered region successively fills up with IL species in the
9 disordered 2D phase, i.e., the phase boundary changes with time. As discussed before, the
10 stripy features in the fast scan direction are presumably due to highly mobile adsorbed IL
11 species in a 2D liquid phase.⁴⁶⁻⁴⁸ Thus, there is exchange of adspecies at the boundary
12 between disordered 2D phase and 2D liquid. In contrast to the 2D crystalline phase, the
13 adsorbed species in the disordered 2D phase are not fully immobile; infrequent molecular
14 jumps are observed. We assume that both the interaction with the steps and the absence of
15 strongly attractive adsorbate-adsorbate interactions prevent the adlayer from ordering on small
16 terraces. As described before, even at low temperatures of around 100 K we did not observe
17 small islands of the ordered [BMP][TFSA] adlayer phase on Ag(111), but just larger ordered
18 areas.

19
20
21 In similar time-resolved measurements we could resolve the 2D melting of the 2D
22 crystalline phase. The results were acquired by applying “slow” linear heating ramps (~0.5
23 K/min), starting from an initial temperature of around 100 K. This way, we could reproducibly
24 determine a 2D melting temperature of the ordered 2D crystalline phase of 180 ± 10 K. Above
25 180 K, we observed stripy features, which are attributed to a 2D liquid adlayer (SI IV). The
26 ‘melting’ temperature of the 2D glass phase is presumably slightly lower than that of the 2D
27 crystalline phase; an accurate value can not be given. However, extrapolating the intrinsic
28 motion in this phase at 100 K to higher temperatures, a lower melting point compared to the
29 ordered 2D crystalline phase seems plausible. In a more general sense, the presence of long-
30 range ordered islands with a low melting point and their equilibrium with a surrounding 2D
31
32
33
34
35
36
37
38
39
40
41
42
43
44
45
46
47
48
49
50
51
52
53
54
55
56
57
58
59
60

1
2
3 liquid phase point to weakly attractive adsorbate – adsorbate interactions and a low barrier for
4
5 surface diffusion.
6

7
8 We now focus on the structure of the stable, ordered 2D crystalline phase. The high
9
10 resolution STM image of this phase in Figure 4a resolves an alternating sequence of pairs of
11
12 longish protrusions and round dots, where the latter are indicated by symbols in the STM
13
14 image. The dimensions of the unit cell are $|a| = 2.3 \pm 0.1$ nm and $|b| = 1.1 \pm 0.1$ nm and
15
16 $\alpha = 95 \pm 3^\circ$, with two dots and four longish protrusions per unit cell. Hence, the ratio of dots
17
18 to longish protrusions is 1 : 2 (Figure 4b). The pairs of longish protrusions as well as the dots
19
20 are aligned along one of the lattice vectors, with always one line of dots followed by one line
21
22 of longish protrusions. Between successive lines of longish protrusion their orientation
23
24 changes by $\sim 120^\circ$. This together with the observation of three rotational domains indicate that
25
26 the adlayer is symmetrically aligned with the Ag(111) surface, with the lines oriented along
27
28 the close packed directions of the Ag(111) surface.
29
30

31
32 Despite of the detailed structural information gained from the STM data, it is not possible to
33
34 identify the origin of the different features from these images alone. Further insight comes
35
36 from DFT-D calculations, which provide a detailed understanding of the anion-cation
37
38 adsorption complex and can explain the appearance in STM images for the given tunneling
39
40 conditions. However, both the cation and the anion have many possible conformations at the
41
42 surface due to rotation around C-C, N-C or S-C single bonds. In order to reduce the number of
43
44 possible starting conformations of the adsorption structure of the IL pair, we will first analyze
45
46 the most stable conformations of the isolated cation and the isolated anion. Especially for the
47
48 cation, the orientation of the alkyl chain may have a strong impact on the appearance in the
49
50 STM image and/or the packing density of the molecules at the surface. In the gas phase, the 5-
51
52 membered ring of $[\text{BMP}]^+$ adopts an envelope conformation in which the butyl group either
53
54 occupies the axial position (as shown in Figure 5a) or the equatorial position, i.e., the butyl
55
56 group is either perpendicular or parallel to the cyclopentane ring. For the isolated cation, the
57
58
59
60

1
2
3 equatorial position is about 18 meV more stable. As this energetic difference is rather small
4
5 and the actual conformation at the surface may depend on the coverage, the conformer with
6
7 the butyl group in the axial position was considered as well. On the other hand, it should also
8
9 be considered that the axial position, with the butyl group sticking up when the imidazol ring
10
11 is parallel to the surface, would allow a higher packing density.
12

13
14 To identify the most probable locations for the attachment of an anion, we evaluated the
15
16 electrostatic potential at an isosurface of the total charge density of the [BMP]⁺ cation (see
17
18 Figure 5a). The blue regions reveal the most positive electrostatic potential experienced by a
19
20 positive test charge, i.e., they indicate the regions where a negative (partial) charge would
21
22 attach preferentially. In contrast, the red regions reveal the least positive electrostatic potential
23
24 a positive test charge would experience. Accordingly, the anion most probably attaches in the
25
26 middle of the triangle formed by the hydrogen atoms of the α -C-atoms.
27
28

29
30 For the isolated [TFSA]⁻ anion, two stable conformations are obtained. In the first one, the
31
32 CF₃ groups are both located above (or below) the S-N-S plane, which is subsequently denoted
33
34 as *cis*-conformation. In the second conformation, which is accordingly termed as *trans*-
35
36 conformation, one CF₃ groups is above and the other one below the S-N-S plane. The *trans*-
37
38 conformer is about 40 meV more stable than the *cis*-conformer. Additionally, the rotational
39
40 barrier that needs to be overcome for transferring from the one into the other conformer is
41
42 rather small, in the range of 50-100 meV. Sobota et al. reported for an imidazolium based
43
44 ionic liquid that in the multilayer both the *cis*- and the *trans*-conformers of [TFSA]⁻ coexist,
45
46 whereas in the monolayer the *cis*-conformer is found on a Al₂O₃/NiAl(110) support.²⁹
47
48 Considering the adsorbed ionic liquid rather than an individual anion, two additional factors
49
50 may affect the relative stability of the respective conformers: the interaction with the counter
51
52 ion, here the cation, and the interaction with the surface. Due to these interactions, even quite
53
54 different conformers might be involved in the most stable complexes. Similar to the procedure
55
56 for the [BMP]⁺ cation, the electrostatic potential is calculated at and mapped onto an
57
58
59
60

1
2
3 isosurface of the total charge density of the [TFSA]⁻ anion (see Figure 5b) to estimate possible
4 positions of attached cations. For both the *cis*- and the *trans*-conformation (not shown), the
5 most attractive regions for positive charges (red regions) are within the S-N-S plane. In order
6 to probe the possible changes in the stability induced by an attached cation, we choose the
7 alkali metal ion Li⁺ as a simple model. Both the *cis*- and the *trans*-conformers of [TFSA]⁻ lead
8 to stable complex structures with the alkali metal cation. Due to the similar stabilization of
9 both [TFSA]⁻ conformers upon interaction with the cation, the *trans*-conformer is more stable
10 than the *cis*-conformer also in a cation-anion complex.
11
12
13
14
15
16
17
18
19

20
21 To elucidate effects resulting from the interaction with the substrate, we first explore the
22 adsorption of [TFSA]⁻ on Ag(111). In that case, the *trans* conformer leads to the most stable
23 adsorption structure, being about 0.2 eV more stable than the metastable *cis*-conformer. Both
24 the *cis*- and the *trans*-conformer adsorb with their respective dipole moment aligned normal to
25 the surface, with the negatively charged end of the molecule oriented towards the surface. The
26 adsorption distances of both conformers are comparable as well. The distance between the
27 average z-position of the O-atoms (only 2 atoms are taken into account in the case of the
28 *trans*-conformer) and the Ag-atoms of the topmost surface layer is 2.472 Å and 2.717 Å for
29 the *trans*- and *cis*-conformer, respectively.
30
31
32
33
34
35
36
37
38
39
40

41 Although we have worked out stable anion and cation conformations in the gas phase and at
42 the surface, there are still many possibilities for the structure at the surface. In the following
43 we restrict the discussion to only one possibility that has been found to be theoretically stable
44 and that is compatible with our experimental results. A valuable experimental input is that the
45 appearance and the size of the unit cell of [BMP][TFSA] on Ag(111) and others which we
46 observed for related ILs with different alkyl groups ([EMIM][TFSA], [OMIM][TFSA]) are
47 nearly identical, which is a strong indication that the alkyl chain of the cation adopts the axial
48 position, pointing towards the vacuum. Furthermore, there is also some information about the
49 adsorption structure of similar ionic liquids on Au(111) by angle resolved x-ray photoelectron
50
51
52
53
54
55
56
57
58
59
60

1
2 spectroscopy (ARXPS).²⁸ According to the ARXPS measurements for [MMIM][TFSA]
3 adsorbed on Au(111), both the cation and the anion are in contact with the surface.²⁸ The
4 authors of the above study also proposed that the oxygen atoms of adsorbed [TFSA]⁻ are
5 pointing towards the surface, whereas the fluoromethyl groups are directed towards the
6 vacuum. These experimental findings suggest that the butyl group of adsorbed [BMP]⁺ adopts
7 the axial position and the *cis*-conformer of adsorbed [TFSA]⁻ is present in the monolayer of
8 [BMP][TFSA] on Ag(111). Albeit, as shown above, both this conformation itself and its
9 adsorption are less stable than that of the *trans*-conformer, it might still lead to a more stable
10 structure of the total adsorption complex due to more favorable adsorbate – adsorbate
11 interactions, as the electrostatic potential of [TFSA]⁻ is most negative in the S-N-S plane,
12 which in turn is parallel to the surface in case of the *cis*-conformer. Thus, the interactions with
13 neighboring cations are expected to be stronger than in the case of the *trans*-conformer where
14 the S-N-S-plane (and thus the most negative electrostatic potential) is normal to the surface.
15
16
17
18
19
20
21
22
23
24
25
26
27
28
29
30
31

32 When looking at the structure of the adsorption complex (see Figure 5c) and comparing it to
33 that of pure adsorbed [TFSA]⁻ (in the *cis*-conformation), there are barely any differences: the
34 anion is only slightly further away from the surface (about 0.10 Å) than for the pure adsorbed
35 [TFSA]. The adsorption energy with respect to the ionic liquid pair in the gas phase is 1.30
36 eV. However, 95% of the adsorption energy is due to dispersion interactions, i.e., all other
37 interactions (electrostatic interactions, covalent bonding) only lead to an adsorption energy of
38 0.06 eV. The charge density difference map (Figure 5d) provides an insight into the electronic
39 changes occurring upon adsorption. Upon adsorption, electrons are shifted from the blue
40 regions to the red regions. As expected, there is a depletion of electron charge in the region
41 between the anion and the surface, whereas it is enhanced in the region between the surface
42 and the cation. Thus, the ion pair induces a lateral dipole at the surface which is opposite in
43 sign to the dipole generated by the two adsorbed ions. For the understanding of the adsorption
44 bond it would be interesting to know whether the enhanced/depleted electron density is due to
45
46
47
48
49
50
51
52
53
54
55
56
57
58
59
60

1
2
3 a charge transfer from the surface to the ionic liquid (and vice versa) or whether it is due to
4 polarization effects within the individual components. This could tell us whether the charge
5 remains at the ionic liquid or whether there is a significant charge transfer to / from the
6 adsorbed species. In the first case, there will be considerable electrostatic adsorbate-adsorbate
7 interactions, which lead to the formation of an ordered structure, in the second case ordering
8 has to occur via different mechanisms, e.g., weaker dipolar interactions or van der Waals
9 interactions between adsorbates, and indirect (surface mediated) adsorbate-adsorbate
10 interactions. However, it is hard to distinguish between charge transfer and polarization
11 effects as the assignment of charges to individual components mainly depends on the position
12 of the border between them. Therefore, different methods for charge analysis that are based on
13 different dividing schemes can lead to very diverse results. In order to get at least a rough
14 estimate of the charge distribution within the system, we used the Bader charge analysis. We
15 found that the charges of the cation and the anion hardly change upon adsorption on Ag(111).
16 This is in agreement with the rather small interaction energy of 0.06 eV if dispersive
17 interactions are excluded, i.e., with the absence of any significant covalent bond formation.

18
19
20
21
22
23
24
25
26
27
28
29
30
31
32
33
34
35
36 In Figure 6 we show simulated STM images of two possible adsorption structures with
37 comparable adsorption energy. These simulations suggest that the experimentally observed
38 dots in the high-resolution STM images correspond to the cations. This seems to be the only
39 way to explain the large corrugation of the isosurface of the partial electronic density
40 contributing to the STM image. The longish protrusions could be related to the adsorbed
41 anion. It seems that each anion leads to two longish protrusions, each of them stemming from
42 2 F-atoms of the fluoromethyl groups. This could explain the ratio of 1:2 of dots to longish
43 protrusions. Furthermore, different voltages in between -0.3 V and -1.5 V have been studied;
44 however no voltage dependency could be observed.

45
46
47
48
49
50
51
52
53
54
55
56
57 According to the STM simulations, the anion-cation pairs in the ordered 2D crystalline
58 phase are depicted in the high-resolution STM image in Figure 6b on the right hand side by
59
60

1
2
3 superimposed dots and longish protrusions. Apparently, the IL structure is formed by an
4
5 alternating sequence of rows in which the anion-cation pairs exhibit the same azimuthal
6
7 orientation. In this herringbone-type arrangement, the azimuthal orientation of the ion pairs
8
9 changes by 120° between subsequent rows. The unit cell is included as well; it contains two
10
11 dots and four longish protrusions, which are now identified as two “anion-cation pairs” with
12
13 different orientations. It should be noted that the term adsorbed ion pair is in so far misleading
14
15 as we have no indication for a structure dominated by strongly attractive interactions between
16
17 intact ion pairs and weak interactions between neighbored ion pairs. Instead, Figure 6b clearly
18
19 demonstrates that the spacing between anions and cations is rather similar, resembling a 2D
20
21 ion crystal. Furthermore, the layer is rotationally aligned with the substrate, possibly due to the
22
23 interaction of the oxygen atoms of the anion with the surface.
24
25
26
27
28

29 **4. Conclusions**

30
31 Having investigated the interaction of [BMP][TFSA] with Ag(111) and the structure
32
33 formation in the adlayer by variable temperature STM measurements and DFT based
34
35 calculations, we arrive at the following results and conclusions:
36
37

- 38 1. Following deposition of [BMP][TFSA] on Ag(111) at room temperature and cool-down
39
40 to around 100 K, we observed the coexistence of an ordered 2D crystalline phase, a
41
42 disordered 2D glass phase and a 2D liquid phase. The 2D glass phase was solely
43
44 observed on small Ag(111) terraces ($d \approx 10$ nm), and is probably induced by the
45
46 interaction with the steps and the lateral confinement. On large Ag(111) terraces, long-
47
48 range ordered and homogenous domains are formed without any internal domain
49
50 boundaries.
51
- 52 2. Variable temperature STM measurements reveal melting of the ordered 2D crystalline
53
54 phase at 180 ± 10 K.
55
56
57
58
59
60

- 1
2
3 3. Dynamic STM measurements at around 100 K resolve exchange of adspecies at the
4 phase boundaries 2D crystalline phase | 2D liquid and disordered 2D glass | 2D liquid.
5
6 While the interior of the ordered 2D crystalline phase is stable over time, infrequent
7
8 molecular jumps are observed in the 2D glass phase.
9
10
- 11 4. The fact that we observe long-range ordered domains with a low 2D melting point and
12 an equilibrium between the 2D crystalline phase and the 2D liquid phase points to
13
14 weakly attractive adsorbate-adsorbate interactions and a low surface diffusion barrier.
15
16
- 17 5. DFT-D calculations reveal a stable adsorption complex for one IL pair with the anion
18 and the cation laterally placed side by side. The butyl group of the cation points towards
19
20 the vacuum and the anion exhibits a *cis*-conformation of the S-N-S plane, with the SO₂
21
22 groups binding to the surface and the trifluoromethyl groups pointing towards the
23
24 interface IL | vacuum. STM simulations agree with the molecular features in high-
25
26 resolution STM images, allowing us to identify anions and cations. In addition, the
27
28 calculations show that the charge remains at the ionic liquid and the interaction with the
29
30 substrate mainly occurs almost exclusively via dispersion interactions and weak
31
32 electrostatic (dipole-induced dipole) interactions. The ordered 2D crystalline phase is
33
34 stabilized by weakly attractive electrostatic interactions between the positive and
35
36 negative charges of the adsorbed ions. Finally, the layer is rotationally aligned with the
37
38 substrate surface, probably due to the interaction of the oxygen atoms of the anion with
39
40 the surface.
41
42
43
44
45
46
47
48
49
50
51
52
53
54
55
56
57
58
59
60

5. Figures

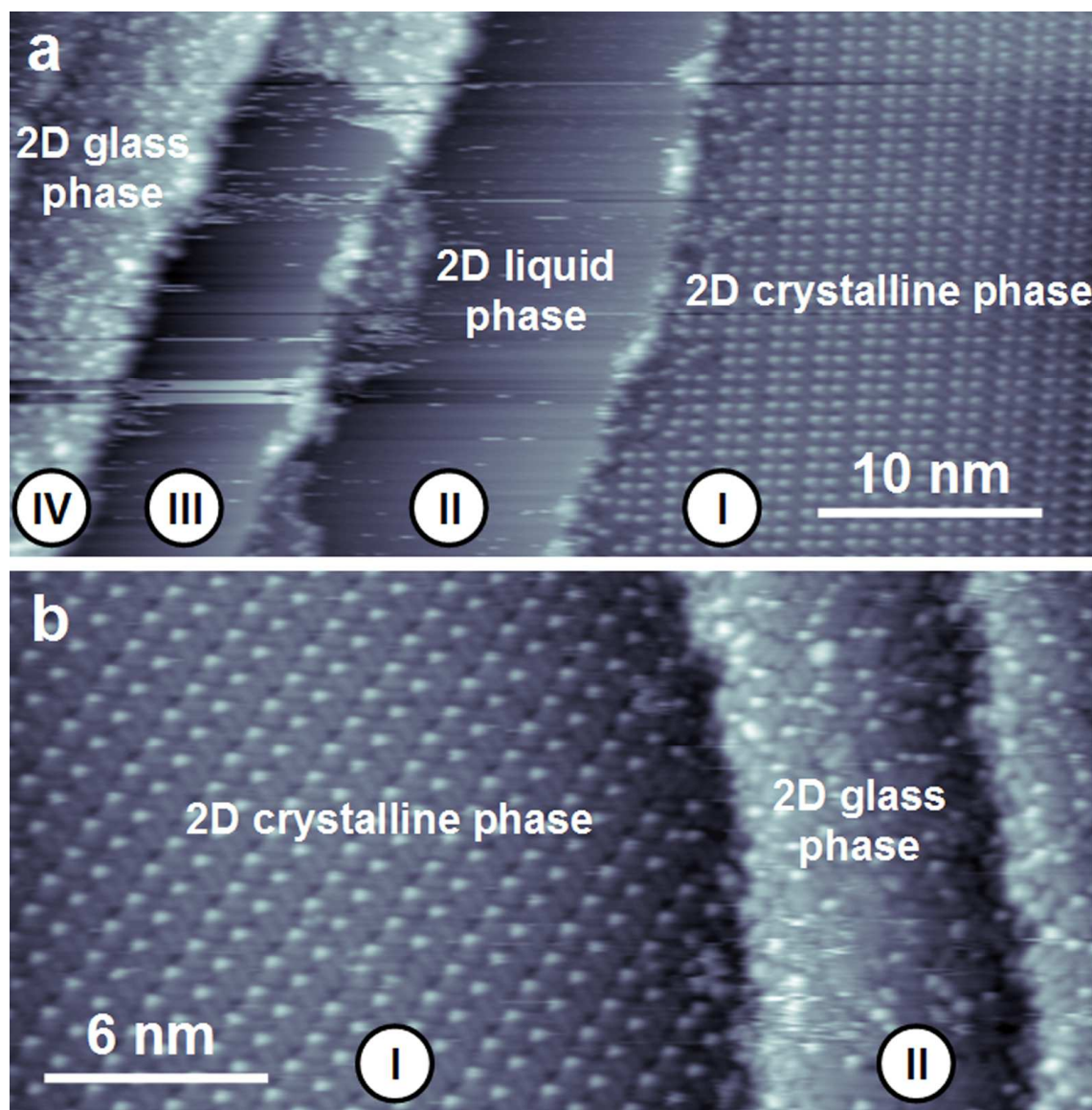


Figure 1. Constant current STM images of [BMP][TFSA] on Ag(111) recorded at ~ 100 K. (a) The STM image at sub-monolayer coverage shows four silver terraces (indicated by numbers). Both an ordered 2D crystalline phase on the large Ag terrace and a disordered 2D glass phase on small Ag terraces (width ~ 10 nm) could be resolved. (b) At monolayer coverage, the large terrace is occupied by the ordered 2D crystalline, while small terraces are covered by the disordered 2D glass phase ((a) $U_t = -0.42$ V, $I_t = 110$ pA, (b) $U_t = -0.37$ V, $I_t = 130$ pA).

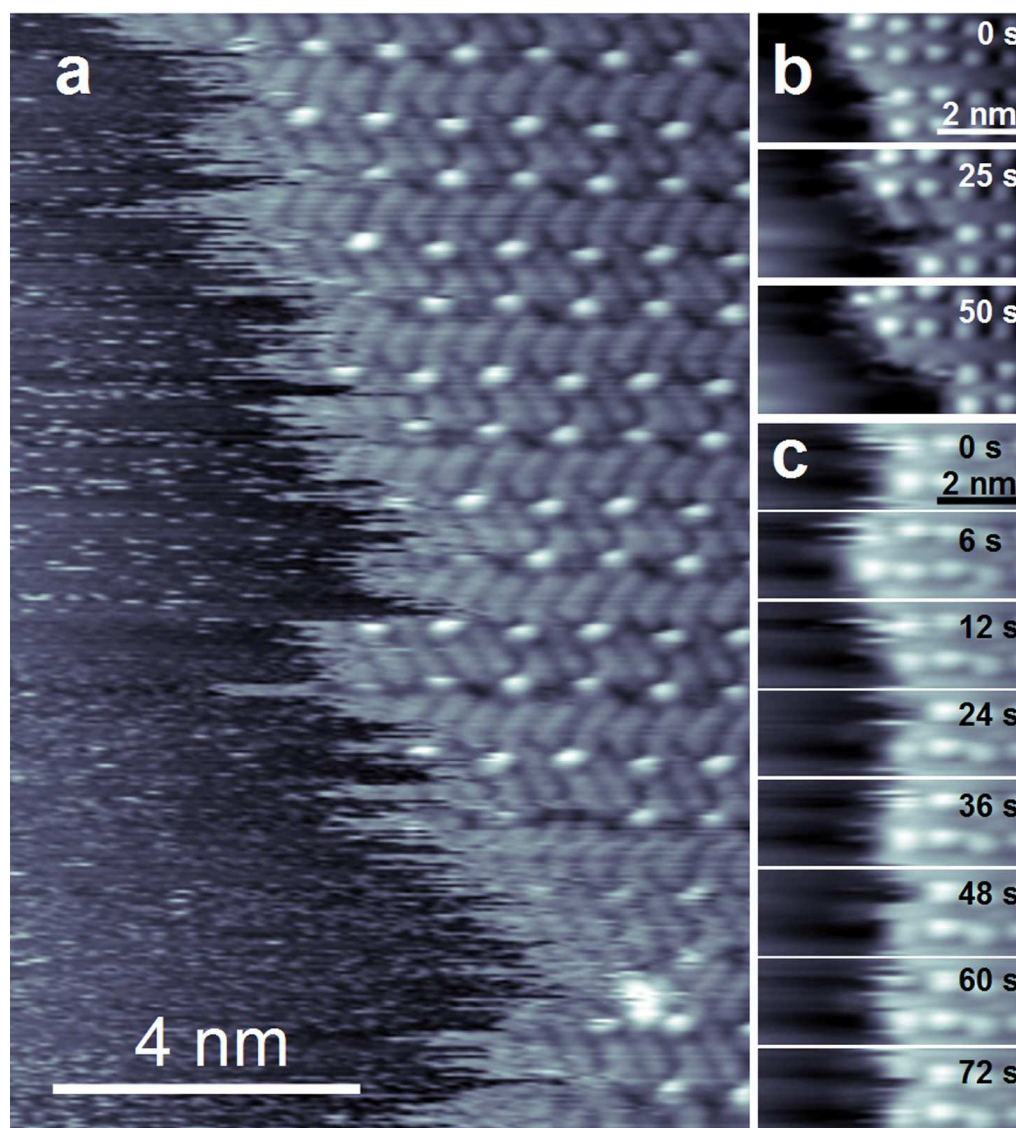


Figure 2. Constant current STM images of [BMP][TFSA] on Ag(111) recorded at ~ 100 K. (a) STM image of the ordered 2D crystalline phase exhibiting frizzy features at the phase boundary to the 2D liquid phase, which are presumably due to exchange of adsorbed IL species at the phase boundary between 2D solid and 2D liquid. Time sequences of STM images with an image to image time of ~ 25 s in (b) and of ~ 6 s in (c) illustrate the dynamic changes at the phase boundary ((a) $U_t = -0.33$ V, $I_t = 150$ pA), (b) $U_t = -1.2$ V, $I_t = 90$ pA, (c) $U_t = -1.2$ V, $I_t = 100$ pA).

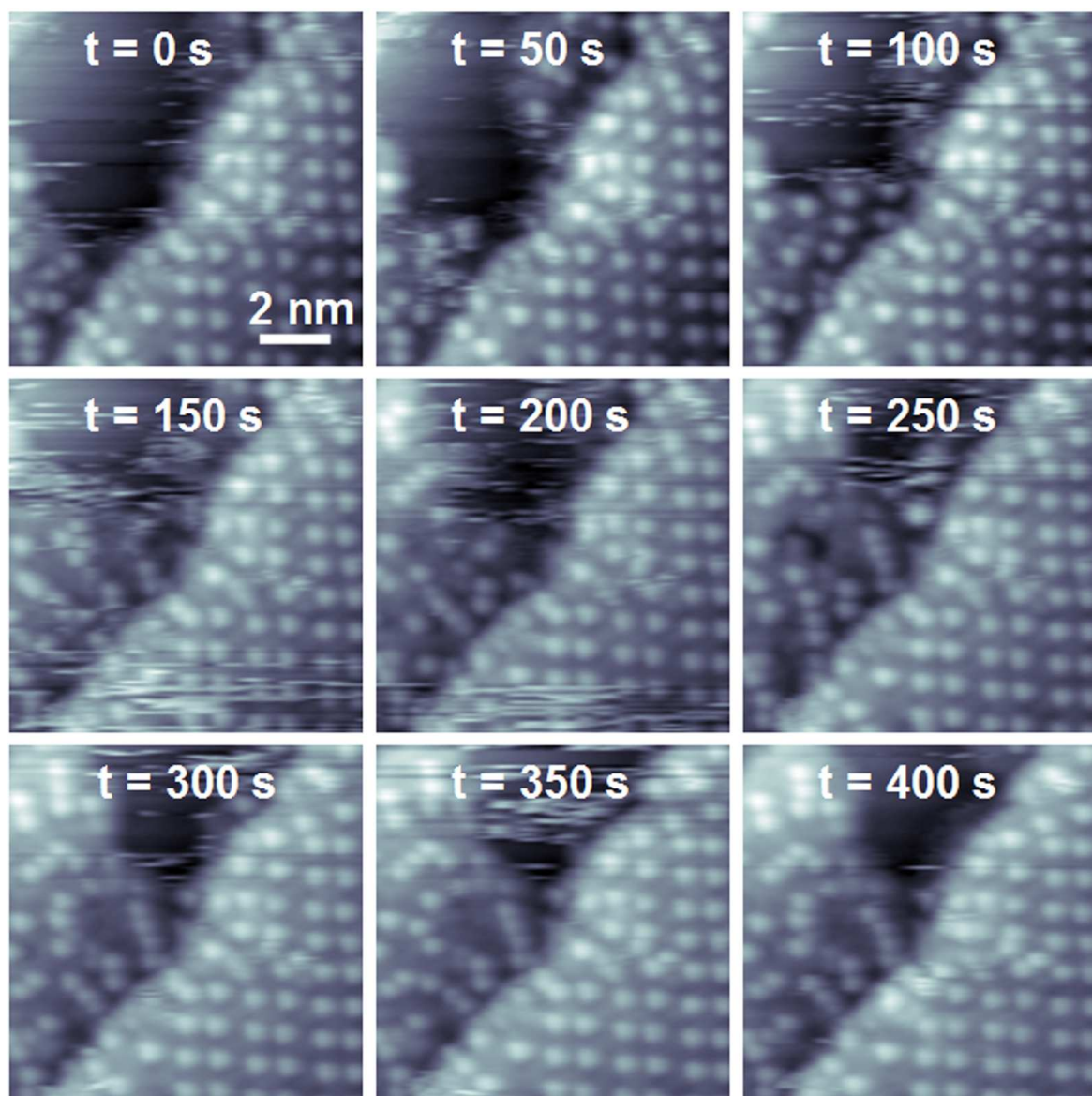


Figure 3. STM time sequence of [BMP][TFSA] on Ag(111) recorded at ~ 100 K. On the left Ag terrace, the phase boundary between disordered 2D glass and 2D liquid is monitored with a time interval from image to image of ~ 12 s (every fourth image is shown). Both the stripy features close to the phase boundary and the gradually changing phase boundary illustrate the exchange of adsorbed IL species between the phases. The right terrace is partly covered by a stable 2D crystalline phase ($U_t = -0.86$ V, $I_t = 50$ pA).

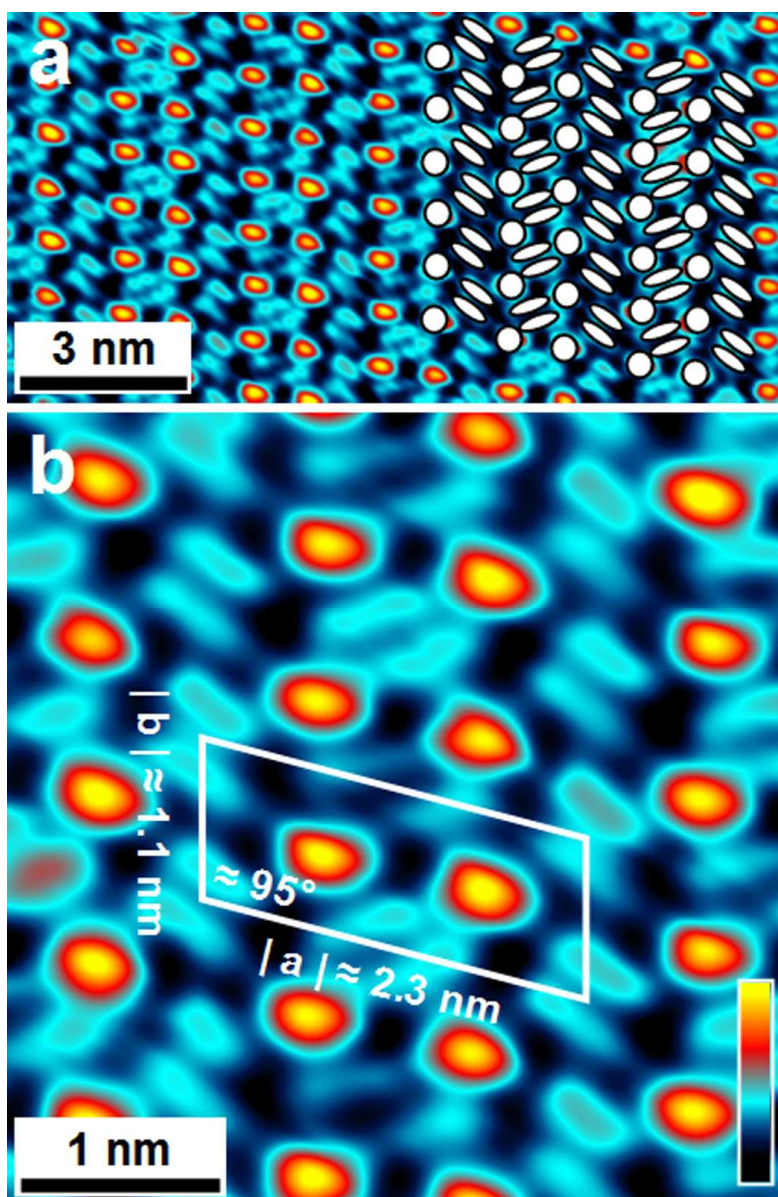


Figure 4. High resolution STM images of [BMP][TFSA] on Ag(111) recorded at $\sim 100 \text{ K}$. (a) High-resolution STM image of the ordered 2D crystalline phase; on the right hand side dots and longish protrusions are superimposed on the image. (b) Enlarged STM image highlighting the structure of the ordered 2D crystalline phase. The unit cell is included, which contains two dots and four longish protrusions ($U_t = -1.32 \text{ V}$, $I_t = 110 \text{ pA}$).

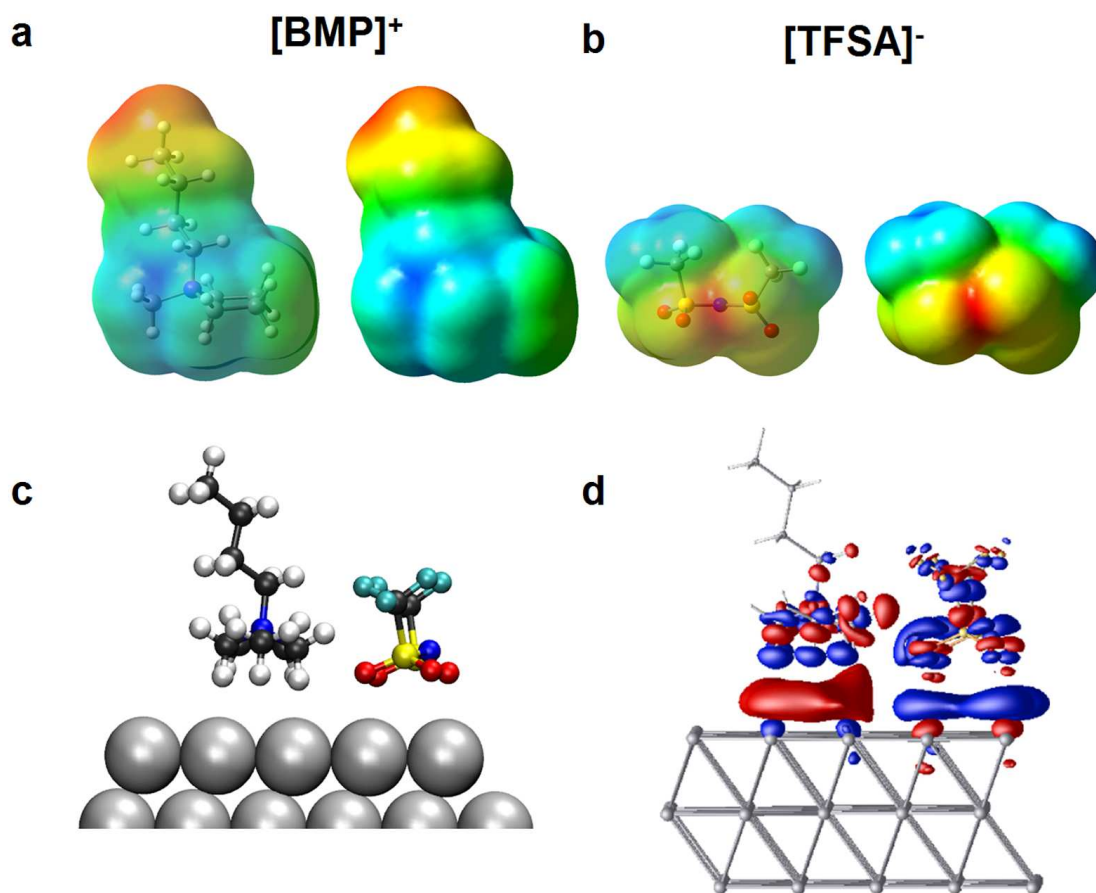


Figure 5. Electrostatic potential at an electron charge isosurface (isosurface charge density $4 \times 10^{-4} e/\text{bohr}^3$) of (a) [BMP]⁺ (view onto the C_{butyl}-N-C_{methyl} plane) and (b) [TFSA]⁻ (view along the S-N-S plane). Red regions refer to the least positive / most negative electrostatic potential a positive test charge experiences. Blue regions reveal the most positive / least negative electrostatic potential a positive test charge experiences. (c) Side view of the adsorption complex of the ionic liquid ion pair on Ag(111). (d) Isosurfaces ($-0.0058 e/\text{\AA}^3$ (blue) and $+0.0049 e/\text{\AA}^3$ (red)) of the adsorption induced changes in the charge density of [BMP][TFSA] adsorbed on Ag(111). The chosen values for the isosurfaces depict a total electron shift of $0.205 e$ from the blue regions into the red regions.

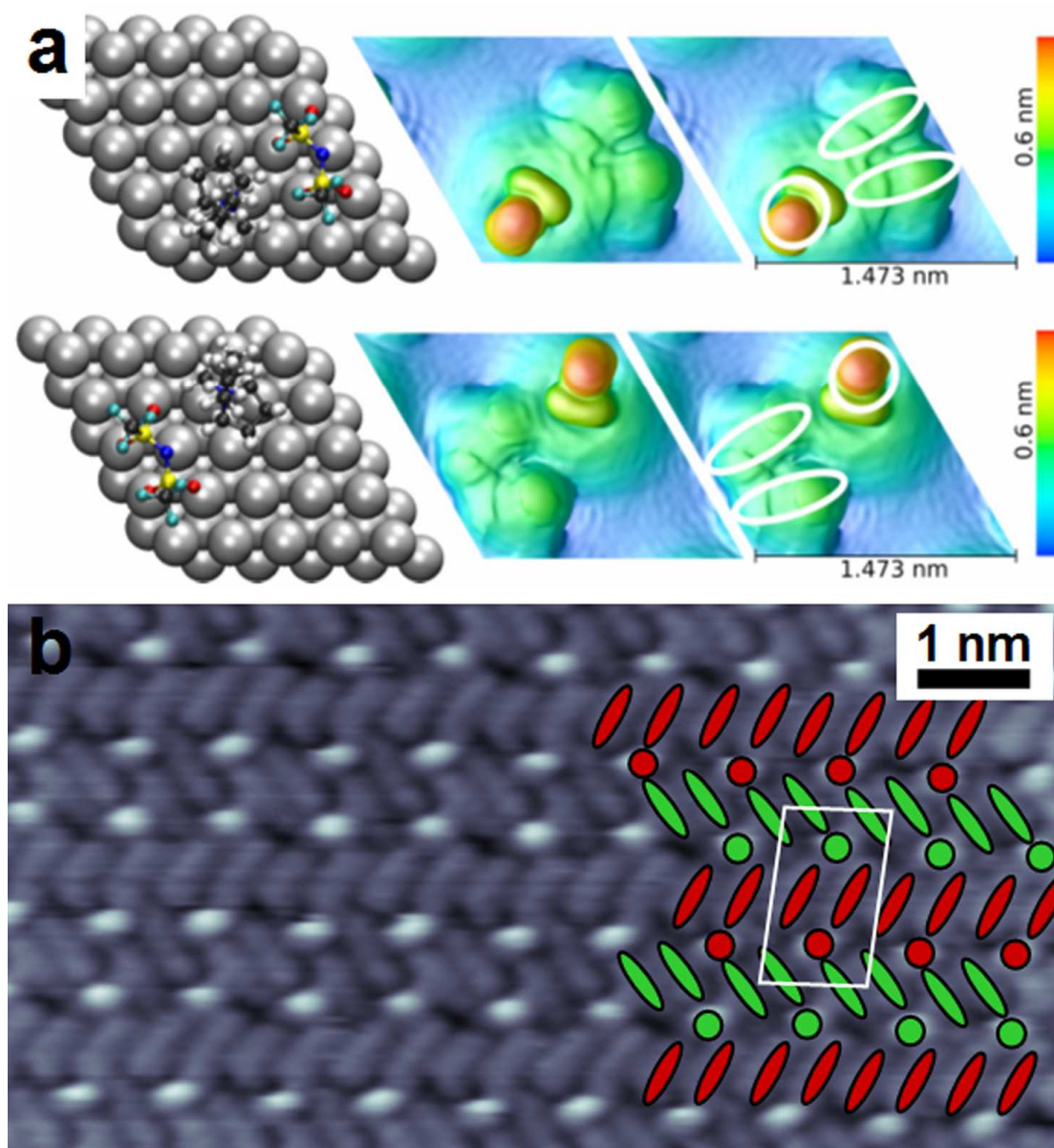


Figure 6. (a) Ball and stick presentation of two mirror symmetric configurations of the adsorbed IL ions together with the corresponding simulated STM images ($U_t = -1.35$ V, isosurface value = $3E-7 e/\text{\AA}^3$) of the adsorption structures of [BMP][TFSA] on Ag(111). The dots and longish protrusions seen in the experimental STM images are indicated on the right. (b) High resolution STM image of the ordered 2D solid phase. On the right hand side, the anion and cations are labeled by schematic drawings, and the unit cell is marked ($U_t = -0.33$ V, $I_t = 150$ pA).

Notes

The authors declare no competing financial interest.

ACKNOWLEDGMENT

B.U. gratefully acknowledges a fellowship by the Fonds der Chemischen Industrie.

REFERENCES

1. Welton, T. Room-Temperature Ionic Liquids. Solvents for Synthesis and Catalysis. *Chem. Rev.* **1999**, *99*, 2071-2084.
2. Ionic Liquids in Synthesis; Wasserscheid, P.; Welton, T. eds; 2 ed., Wiley-VCh: **2008**.
3. Wasserscheid, P.; Keim, W. Ionic Liquids—New "Solutions" for Transition Metal Catalysis. *Angew. Chem. Int. Ed.* **2000**, *39*, 3772-3789.
4. Plechkova, N. V.; Seddon, K. R. Applications of Ionic liquids in the Chemical Industry. *Chem. Soc. Rev.* **2008**, *37*, 123-150.
5. Kuboki, T.; Okuyama, T.; Ohsaki, T.; Takami, N. Lithium-air Batteries Using Hydrophobic Room Temperature Ionic Liquid Electrolyte. *J. Power Sources* **2005**, *146*, 766-769.
6. Armand, M.; Tarascon, J.-M. Building Better Batteries. *Nature* **2008**, *451*, 652.
7. Armand, M.; Endres, F.; MacFarlane, D. R.; Ohno, H.; Scrosati, B. Ionic-liquid Materials for the Electrochemical Challenges of the Future. *Nature Mater.* **2009**, *8*, 621-629.
8. Girishkumar, G.; McCloskey, B.; Luntz, A. C.; Swanson, S.; Wilcke, W. Lithium-Air Battery: Promise and Challenges. *J. Phys. Chem. Lett.* **2010**, *1*, 2193-2203.
9. Steinrück, H.-P.; Libuda, J.; Wasserscheid, P.; Cremer, T.; Kolbeck, C.; Laurin, M.; Maier, F.; Sobota, M.; Schulz, P. S.; Stark, M. Surface Science and Model Catalysis with Ionic Liquid-Modified Materials. *Adv. Mater.* **2011**, *23*, 2571-2587.

- 1
2
3
4
5
6
7
8
9
10
11
12
13
14
15
16
17
18
19
20
21
22
23
24
25
26
27
28
29
30
31
32
33
34
35
36
37
38
39
40
41
42
43
44
45
46
47
48
49
50
51
52
53
54
55
56
57
58
59
60
10. Steinrück, H.-P. Recent Developments in the Study of Ionic Liquid Interfaces Using X-ray Photoelectron Spectroscopy and Potential Future Directions. *Phys. Chem. Chem. Phys.* **2012**, *14*, 5010-5029.
 11. Grimme, S.; Antony, J.; Ehrlich, S.; Krieg, H. A Consistent and Accurate ab Initio Parametrization of Density Functional Dispersion Correction (DFT-D) for the 94 Elements H-Pu. *J. Chem. Phys.* **2010**, *132*, 154104-154119.
 12. Atkin, R.; El Abedin, S. Z.; Hayes, R.; Gasparotto, L. H. S.; Borisenko, N.; Endres, F. AFM and STM Studies on the Surface Interaction of [BMP]TfSA and [EMIm]TfSA Ionic Liquids with Au(111). *J. Phys. Chem. C* **2009**, *113*, 13266-13272.
 13. Endres, F.; Höfft, O.; Borisenko, N.; Gasparotto, L. H. S.; Prowald, A.; Al Salman, R.; Carstens, T.; Atkin, R.; Bund, A.; El Abedin, S. Z. Do Solvation Layers of Ionic Liquids Influence Electrochemical Reactions? *Phys. Chem. Chem. Phys.* **2010**, *12*, 1724-1732.
 14. Atkin, R.; Borisenko, N.; Drüscher, M.; El Abedin, S. Z.; Endres, F.; Hayes, R.; Huber, B.; Roling, B. An in Situ STM/AFM and Impedance Spectroscopy Study of the Extremely Pure 1-Butyl-1-Methylpyrrolidinium Tris(pentafluoroethyl)trifluorophosphate/Au(111) Interface: Potential Dependent Solvation Layers and the Herringbone Reconstruction. *Phys. Chem. Chem. Phys.* **2011**, *13*, 6849-6857.
 15. Drüscher, M.; Borisenko, N.; Wallauer, J.; Winter, C.; Huber, B.; Endres, F.; Roling, B. New Insights Into the Interface Between a Single-Crystalline Metal Electrode and an Extremely Pure Ionic Liquid: Slow Interfacial Processes and the Influence of Temperature on Interfacial Dynamics. *Phys. Chem. Chem. Phys.* **2012**, *14*, 5090-5099.
 16. Gnahn, M.; Berger, C.; Arkhipova, M.; Kunkel, H.; Pajkossy, T.; Maas, G.; Kolb, D. M. The Interfaces of Au(111) and Au(100) in a Hexaalkyl-Substituted Guanidinium Ionic Liquid: an Electrochemical and in Situ STM Study. *Phys. Chem. Chem. Phys.* **2012**, *14*, 10647-10652.

- 1
2
3 17. Smith, E. F.; Rutten, F. J. M.; Villar-Gracia, I. J.; Briggs, D.; Licence, P. Ionic Liquids in
4 Vacuo: Analysis of Liquid Surfaces Using Ultra-High-Vacuum Techniques. *Langmuir* **2006**,
5 22, 9386-9392.
6
7
8
9
10 18. Höfft, O.; Bahr, S.; Himmerlich, M.; Krischok, S.; Schaefer, J. A.; Kempter, V. Electronic
11 Structure of the Surface of the Ionic Liquid [EMIM][Tf₂N] Studied by Metastable Impact
12 Electron Spectroscopy (MIES), UPS, and XPS. *Langmuir* **2006**, 22, 7120-7123.
13
14
15
16 19. Maier, F.; Gottfried, J. M.; Rossa, J.; Gerhard, D.; Schulz, P. S.; Schwieger, W.;
17 Wasserscheid, P.; Steinrück, H.-P. Surface Enrichment and Depletion Effects of Ions
18 Dissolved in an Ionic Liquid: An X-Ray Photoelectron Spectroscopy Study. *Angew. Chem.*
19 *Int. Ed.* **2006**, 45, 7778-7780.
20
21
22
23
24
25 20. Armstrong, J. P.; Hurst, C.; Jones, R. G.; Licence, P.; Lovelock, K. R. J.; Satterley, C. J.;
26 Villar-Garcia, I. J. Vapourisation of Ionic Liquids. *Phys. Chem. Chem. Phys.* **2007**, 9, 982-
27 990.
28
29
30
31
32 21. Souda, R. Glass-Liquid Transition, Crystallization, and Melting of a Room Temperature Ionic
33 Liquid: Thin Films of 1-Ethyl-3-Methylimidazolium Bis[trifluoromethanesulfonyl]imide
34 Studied with TOF-SIMS. *J. Phys. Chem. B* **2008**, 112, 15349-15354.
35
36
37
38
39 22. Deyko, A.; Lovelock, K. R. J.; Corfield, J. A.; Taylor, A. W.; Gooden, P. N.; Villar-Garcia, I.
40 J.; Licence, P.; Jones, R. G.; Krasovskiy, V. G.; Chernikova, E. A.; Kustov, L. M. Measuring
41 and Predicting $\Delta_{\text{vap}}H_{298}$ Values of Ionic Liquids. *Phys. Chem. Chem. Phys.* **2009**, 11, 8544-
42 8555.
43
44
45
46
47
48 23. Lovelock, K. R. J.; Villar-Garcia, I. J.; Maier, F.; Steinrück, H. P.; Licence, P. Photoelectron
49 Spectroscopy of Ionic Liquid-Based Interfaces. *Chem. Rev.* **2010**, 110, 5158-5190.
50
51
52
53 24. Sobota, M.; Schmid, M.; Happel, M.; Amende, M.; Maier, F.; Steinrück, H.-P.; Paape, N.;
54 Wasserscheid, P.; Laurin, M.; Gottfried, J. M.; Libuda, J. Ionic Liquid Based Model
55 Catalysis: Interaction of [BMIM][Tf₂N] with Pd Nanoparticles Supported on an Ordered
56 Alumina Film. *Phys. Chem. Chem. Phys.* **2010**, 12, 10610-10621.
57
58
59
60

- 1
2
3 25. Maier, F.; Cremer, T.; Kolbeck, C.; Lovelock, K. R. J.; Paape, N.; Schulz, P. S.;
4
5 Wasserscheid, P.; Steinrück, H. P. Insights Into The Surface Composition And Enrichment
6
7 Effects of Ionic Liquids and Ionic Liquid Mixtures. *Phys. Chem. Chem. Phys.* **2010**, *12*, 1905-
8
9 1915.
- 10
11 26. Cremer, T.; Wibmer, L.; Calderon, S. K.; Deyko, A.; Maier, F.; Steinrück, H.-P. Interfaces of
12
13 Ionic Liquids and Transition Metal Surfaces-Adsorption, Growth, and Thermal Reactions of
14
15 Ultrathin [C₁C₁Im][Tf₂N] Films on Metallic and Oxidised Ni(111) Surfaces. *Phys. Chem.*
16
17 *Chem. Phys.* **2012**, *14*, 5153-5163.
- 18
19
20 27. Schernich, S.; Laurin, M.; Lykhach, Y.; Steinrück, H.-P.; Tsud, N.; Skála, T.; Prince, K. C.;
21
22 Taccardi, N.; Matolín, V.; Wasserscheid, P.; Libuda, J. Functionalization of Oxide Surfaces
23
24 through Reaction with 1,3-Dialkylimidazolium Ionic Liquids. *J. Phys. Chem. Lett.* **2012**, *4*,
25
26 30-35.
- 27
28
29 28. Cremer, T.; Stark, M.; Deyko, A.; Steinrück, H.-P.; Maier, F. Liquid/Solid Interface of
30
31 Ultrathin Ionic Liquid Films: [C₁C₁Im][Tf₂N] and [C₈C₁Im][Tf₂N] on Au(111). *Langmuir*
32
33 **2011**, *27*, 3662-3671.
- 34
35
36 29. Sobota, M.; Nikiforidis, I.; Hieringer, W.; Paape, N.; Happel, M.; Steinrück, H.-P.; Görling,
37
38 A.; Wasserscheid, P.; Laurin, M.; Libuda, J. Toward Ionic-Liquid-Based Model Catalysis:
39
40 Growth, Orientation, Conformation, and Interaction Mechanism of the [Tf₂N] Anion in
41
42 [BMIM][Tf₂N] Thin Films on a Well-Ordered Alumina Surface. *Langmuir* **2010**, *26*, 7199-
43
44 7207.
- 45
46
47 30. Waldmann, T.; Huang, H.-H.; Hoster, H. E.; Höfft, O.; Endres, F.; Behm, R. J. Imaging an
48
49 Ionic Liquid Adlayer by Scanning Tunneling Microscopy at the Solid | Vacuum Interface.
50
51 *ChemPhysChem* **2011**, *12*, 2565-2567.
- 52
53
54 31. Foulston, R.; Gangopadhyay, S.; Chiutu, C.; Moriarty, P.; Jones, R. G. Mono- and Multi-layer
55
56 Adsorption of an Ionic Liquid on Au(110). *Phys. Chem. Chem. Phys.* **2012**, *14*, 6054-6066.
57
58
59
60

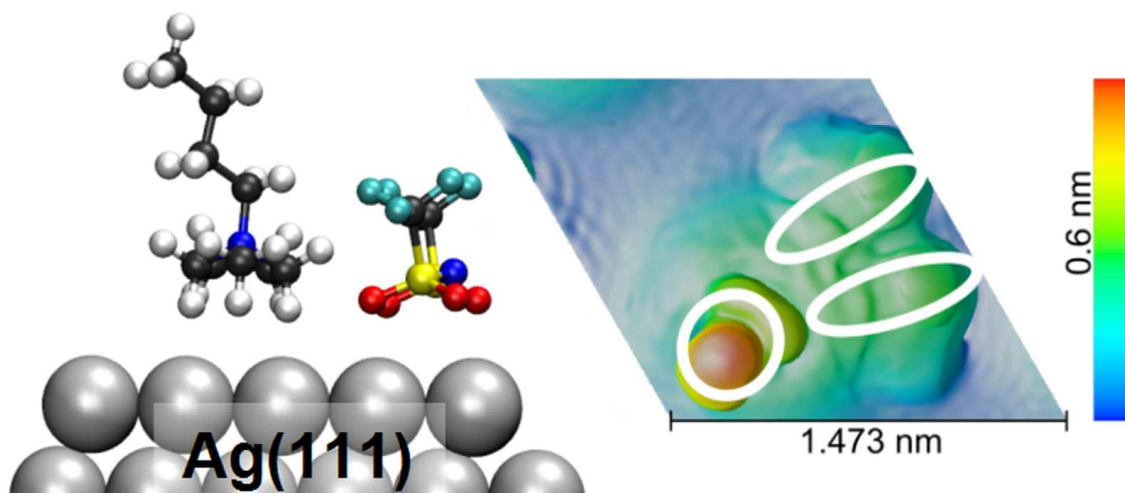
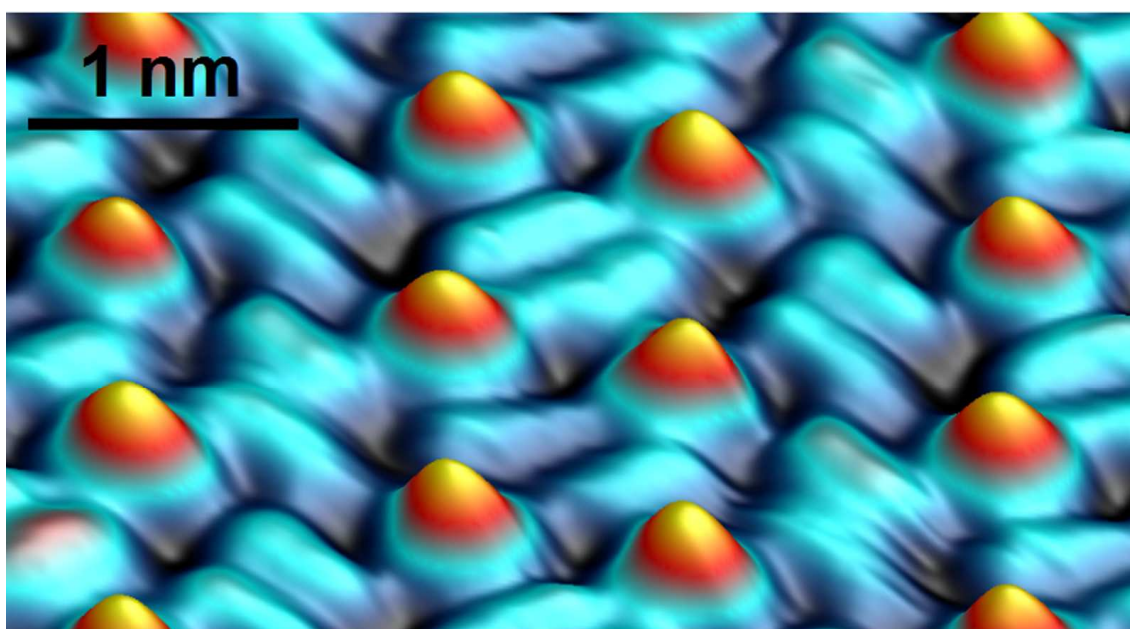
- 1
2
3 32. Perdew, J. P.; Burke, K.; Ernzerhof, M. Generalized Gradient Approximation Made Simple.
4
5 *Phys. Rev. Lett.* **1996**, *77*, 3865-3868.
6
7
8 33. Kresse, G.; Furthmüller, J. Efficiency of ab Initio Total Energy Calculations for Metals and
9
10 Semiconductors Using a Plane-Wave Basis Set. *J. Comp. Mat. Sci.* **1996**, *6*, 15-50.
11
12
13 34. Kresse, G.; Furthmüller, J. Efficient Iterative Schemes for ab Initio Total-Energy Calculations
14
15 Using a Plane-Wave Basis Set. *Phys. Rev. B* **1996**, *54*, 11169-11186.
16
17
18 35. Tonigold, K.; Groß, A. Adsorption of Small Aromatic Molecules on the (111) Surfaces of
19
20 Noble Metals: A Density Functional Theory Study with Semiempirical Corrections for
21
22 Dispersion Effects. *J. Chem. Phys.* **2010**, *132*, 224701-224701-10.
23
24
25 36. Tonigold, K.; Groß, A. Dispersive Interactions in Water Bilayers at Metallic Surfaces: A
26
27 Comparison of the PBE and RPBE Functional Including Semiempirical Dispersion
28
29 Corrections. *J. Comput. Chem.* **2012**, *33*, 695-701.
30
31
32 37. Waldmann, T.; Nenon, C.; Tonigold, K.; Hoster, H. E.; Groß, A.; Behm, R. J. The Role of
33
34 Surface Defects on Large Organic Molecule Adsorption: Substrate Configuration Effects.
35
36 *Phys. Chem. Chem. Phys.* **2012**, *14*, 10726-10731.
37
38
39 38. Blöchl, P. E. Projector Augmented-Wave Method. *Phys. Rev. B* **1994**, *50*, 17953-17979.
40
41
42 39. Kresse, G.; Joubert, D. From Ultrasoft Pseudopotentials to the Projector Augmented-Wave
43
44 Method. *Phys. Rev. B* **1999**, *59*, 1758-1775.
45
46
47 40. Monkhorst, H. J.; Pack, J. D. Special Points for Brillouin-Zone Integrations. *Phys. Rev. B*
48
49 **1976**, *13*, 5188-5192.
50
51
52 41. Tersoff, J.; Hamann, D. R. Theory of the Scanning Tunneling Microscope. *Phys. Rev. B* **1985**,
53
54 *31*, 805-813.
55
56
57 42. Frisch, M. J. et al. Gaussian 09, Revision B.01, Gaussian, Inc., Wallingford CT. Gaussian.
58
59 **2010**.
60

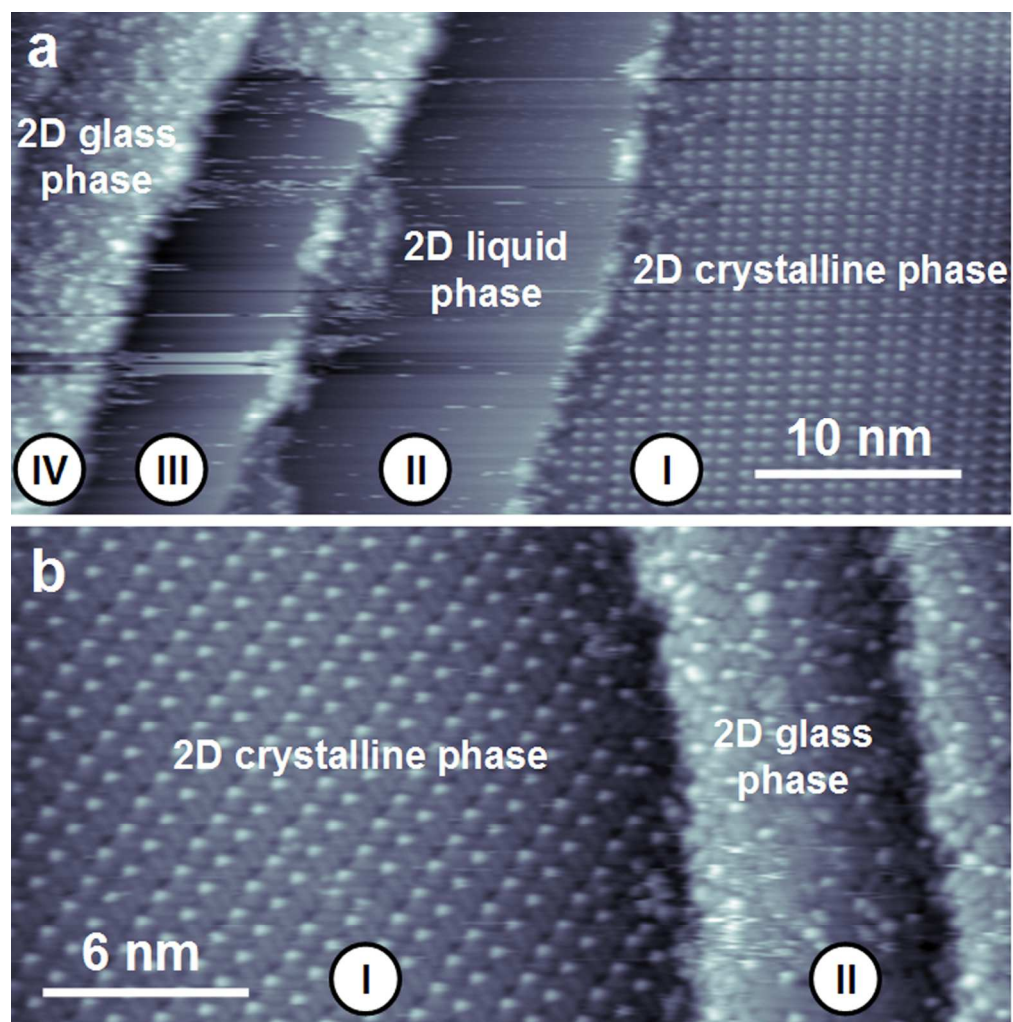
- 1
2
3 43. Dunning Jr., T. H. Gaussian Basis Sets for Use in Correlated Molecular Calculations. I. The
4 Atoms Boron through Neon and Hydrogen. *J. Chem. Phys.* **1989**, *90*, 1007-1023.
5
6
7
8 44. Kendall, R. A.; Dunning, J.; Harrison, R. J. Electron Affinities of the First-Row Atoms
9 Revisited. Systematic Basis Sets and Wave Functions. *J. Chem. Phys.* **1992**, *96*, 6796-6806.
10
11
12 45. Woon, D. E.; Dunning, J. Gaussian Basis Sets for Use in Correlated Molecular Calculations.
13 III. The Atoms Aluminum through Argon. *J. Chem. Phys.* **1993**, *98*, 1358-1371.
14
15
16
17 46. Yanagi, H.; Mukai, H.; Ikuta, K.; Shibutani, T.; Kamikado, T.; Yokoyama, S.; Mashiko, S.
18 Molecularly Resolved Dynamics for Two-Dimensional Nucleation of Supramolecular
19 Assembly. *Nano Lett.* **2002**, *2*, 601-604.
20
21
22
23
24 47. Berner, S.; de Wild, M.; Ramoino, L.; Ivan, S.; Barattoff, A.; Güntherodt, H. J.; Suzuki, H.;
25 Schlettwein, D.; Jung, T. A. Adsorption and Two-Dimensional Phases of a Large Polar
26 Molecule: Sub-Phthalocyanine on Ag(111). *Phys. Rev. B* **2003**, *68*, 115410.
27
28
29
30
31 48. Buchner, F; Zillner, E.; Röckert, M.; Gläbel S.; Steinrück H.-P.; Marbach, H. Substrate-
32 Mediated Phase Separation of Two Porphyrin Derivates on Cu(111). *Chem.Eur. J.* **2011**, *17*,
33 10266-10229
34
35
36
37
38
39
40
41
42
43
44
45
46
47
48
49
50
51
52
53
54
55
56
57
58
59
60

BRIEFS

A pseudo-three-dimensional presentation of a sub-molecularly resolved STM image and the configuration resulting from DFT-D based calculations of the adsorbed ionic liquid [BMP][TFSA] on Ag(111).

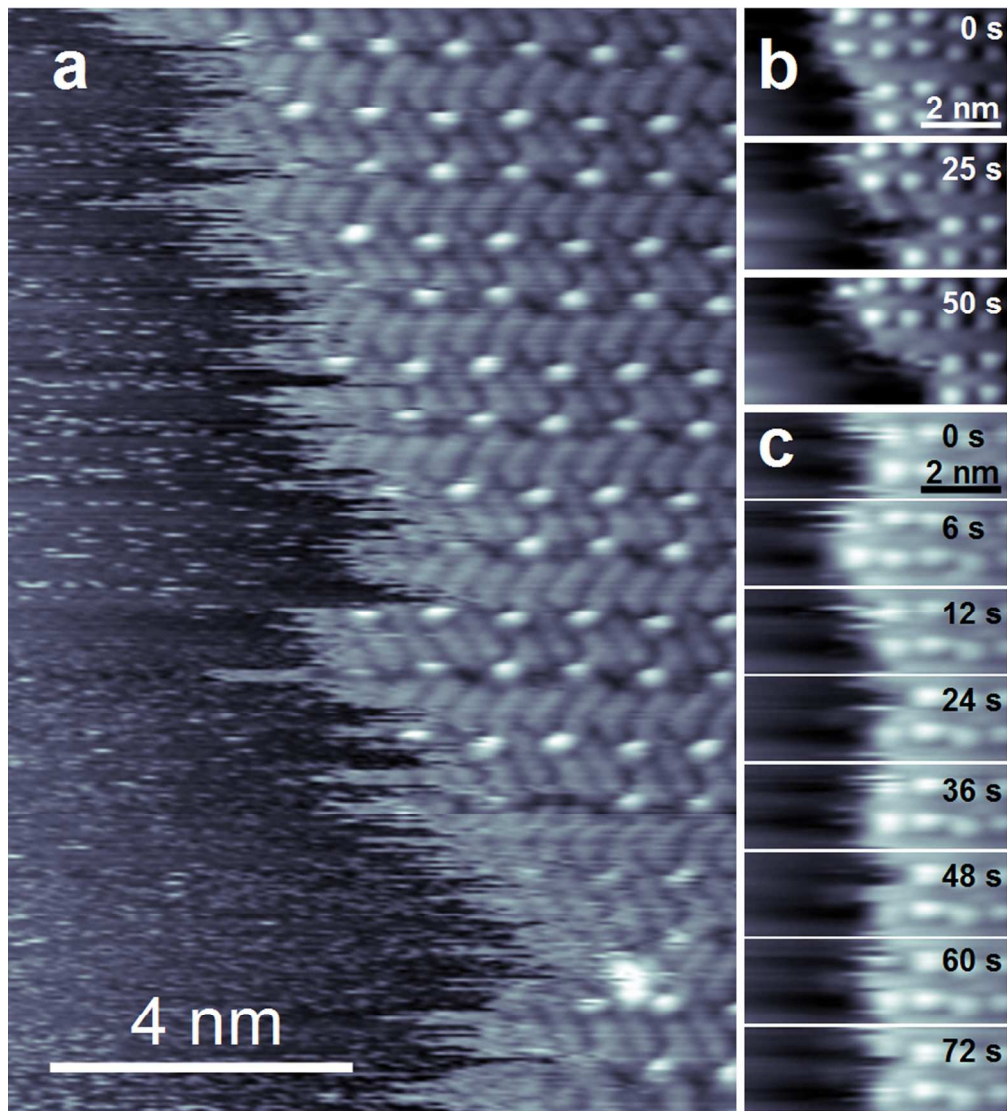
SYNOPSIS



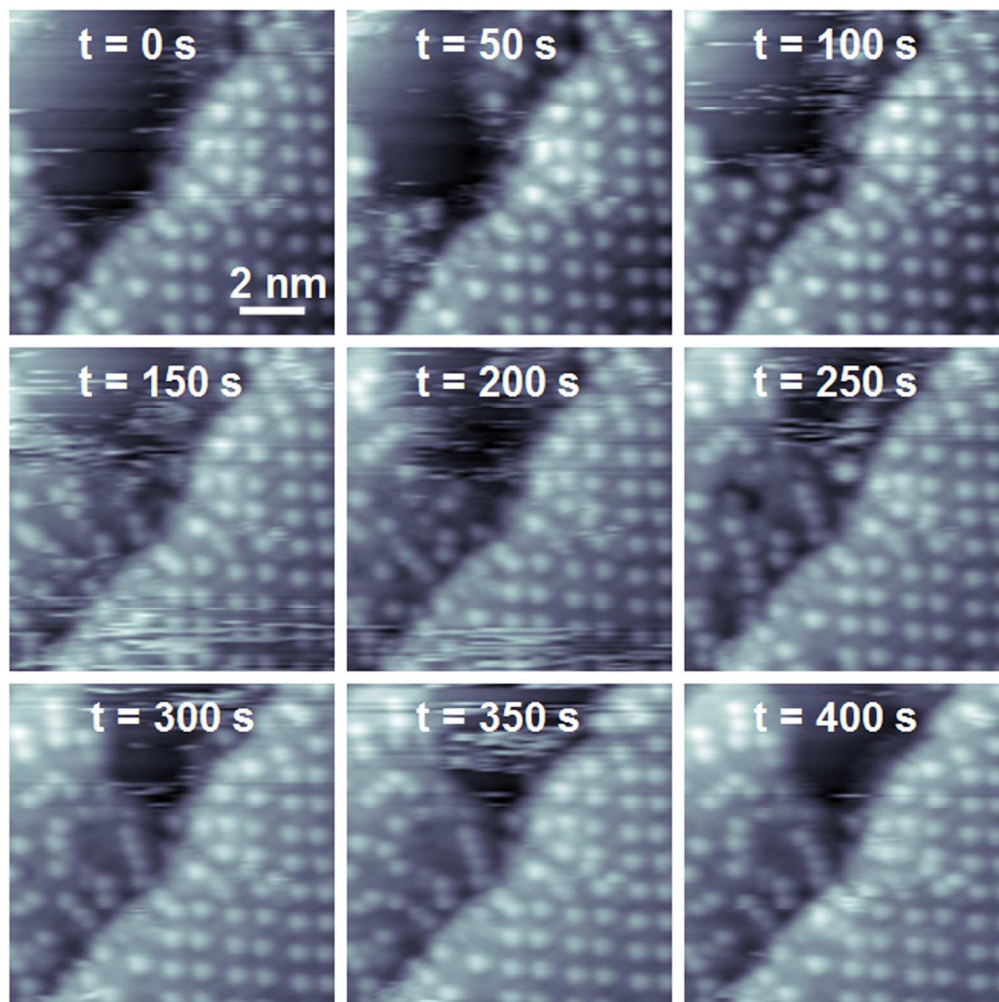


557x564mm (72 x 72 DPI)

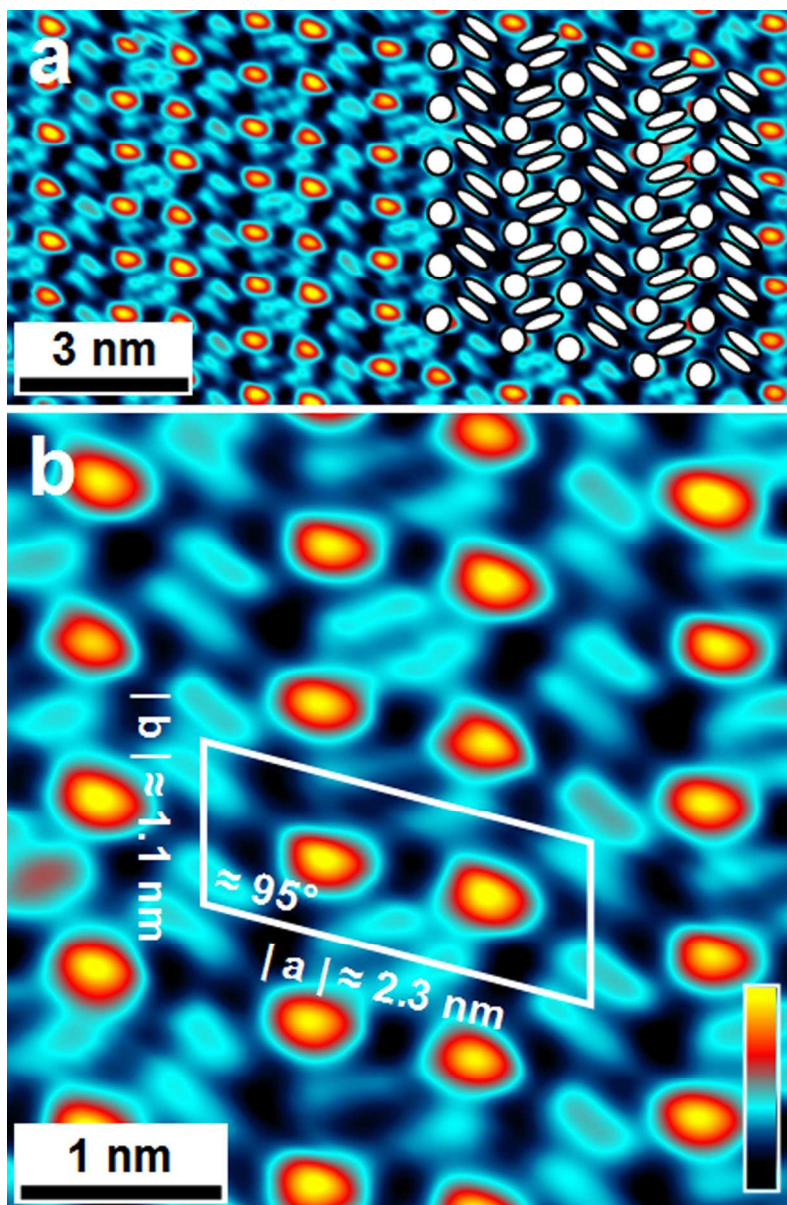
1
2
3
4
5
6
7
8
9
10
11
12
13
14
15
16
17
18
19
20
21
22
23
24
25
26
27
28
29
30
31
32
33
34
35
36
37
38
39
40
41
42
43
44
45
46
47
48
49
50
51
52
53
54
55
56
57
58
59
60



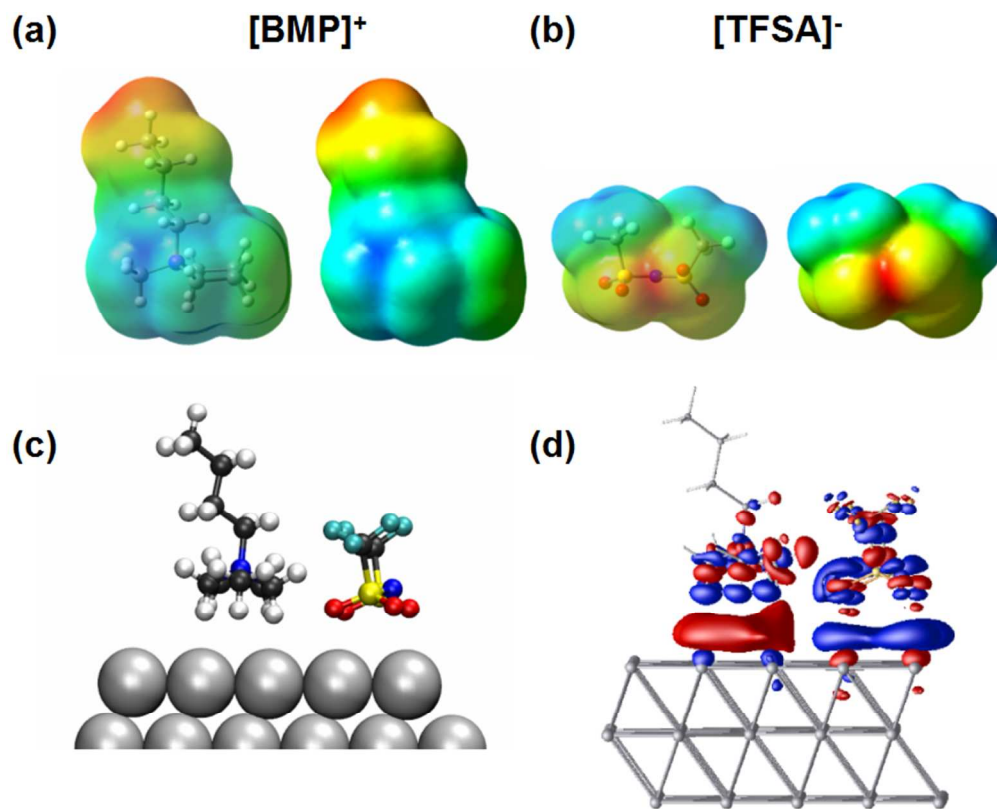
510x564mm (72 x 72 DPI)



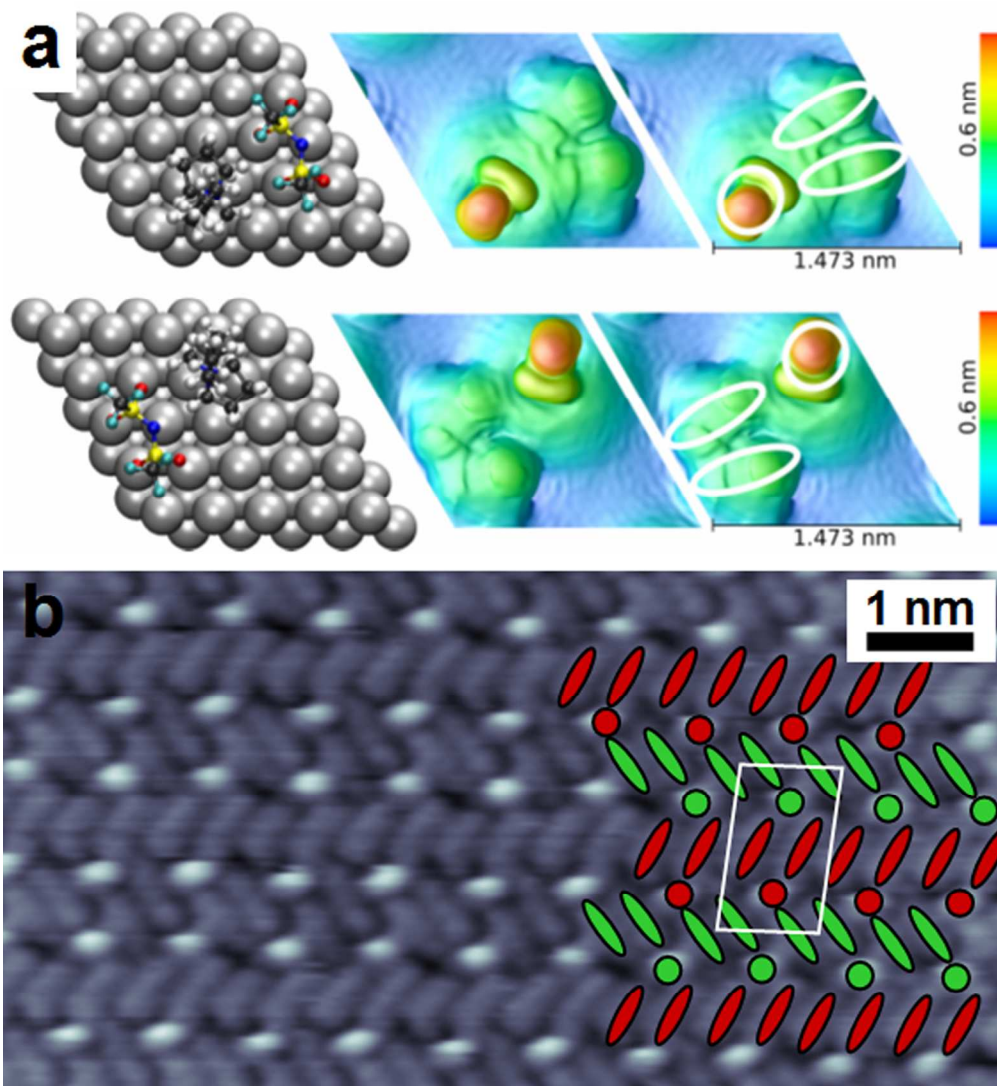
563x564mm (72 x 72 DPI)



370x564mm (72 x 72 DPI)



564x451mm (72 x 72 DPI)



517x564mm (72 x 72 DPI)